Research Article

NMR IN BIOMEDICINE

Received: 29 August 2008, Revised: 18 February 2009, Accepted: 18 February 2009, Published online in Wiley InterScience: 1 May 2009

(www.interscience.wiley.com) DOI:10.1002/nbm.1389

Comparative velocity investigations in cerebral arteries and aneurysms: 3D phase-contrast MR angiography, laser Doppler velocimetry and computational fluid dynamics

Dorothea I. Hollnagel[a,b], Paul E. Summers[c,d], Dimos Poulikakos[b] and Spyros S. Kollias[a]*

In western populations, cerebral aneurysms develop in approximately 4% of humans and they involve the risk of rupture. Blood flow patterns are of interest for understanding the pathogenesis of the lesions and may eventually contribute to deciding on the most efficient treatment procedure for a specific patient. Velocity mapping with phase-contrast magnetic resonance angiography (PC-MRA) is a non-invasive method for performing *in vivo* measurements on blood velocity. Several hemodynamic properties can either be derived directly from these measurements or a flow field with all its parameters can be simulated on the basis of the measurements. For both approaches, the accuracy of the PC-MRA data and subsequent modeling must be validated. Therefore, a realistic transient flow field in a well-defined patient-specific silicone phantom was investigated. Velocity investigations with PC-MRA in a 3 Tesla MR scanner, laser Doppler velocimetry (LDV) and computational fluid dynamics (CFD) were performed in the same model under equal flow conditions and compared to each other. The results showed that PC-MRA was qualitatively similar to LDV and CFD, but showed notable quantitative differences, while LDV and CFD agreed well. The accuracy of velocity quantification by PC-MRA was best in straight artery regions with the measurement plane being perpendicular to the primary flow direction. The accuracy decreased in regions with disturbed flow and in cases where the measurement plane was not perpendicular to the primary flow. Due to these findings, it is appropriate to use PC-MRA as the inlet and outlet conditions for numerical simulations to calculate velocities and shear stresses in disturbed regions like aneurysms, rather than derive these values directly from the full PC-MRA measured velocity field.

Keywords: cerebral aneurysm; MRI; numerical simulation; phase mapping; velocity measurements

INTRODUCTION

Angiographic studies report an incidence of intracranial aneurysms in between 3 and 6% of humans, although autopsy studies suggest a slightly lower occurrence (1,2). The yearly rupture rate of intracranial aneurysms is approximately 2% (3). Treatment approaches are either endovascular coiling or neurosurgical clipping which are invasive procedures with recognized risks of morbidity and mortality (4). In this setting, there is a strong motivation to provide safe and effective treatment for both the symptomatic and silent lesions. Currently, morphological properties provide the basis of pretreatment assessment of such vascular lesions, without reference to the associated hemodynamic abnormalities (5). This ignores the fact that the natural history of aneurysms as well as the course of their treatment are strongly influenced by hemodynamic factors (6,7).

Velocity mapping using phase-contrast magnetic resonance angiography (PC-MRA) is a widely available, non-invasive, and adaptable method for performing *in vivo* blood velocity measurements which can be used for both angiographic and quantitative applications (8–11). By applying cardiac triggering to the image acquisition, four-dimensional maps of the velocity field can be obtained.

* *Correspondence to: S. S. Kollias, Institute of Neuroradiology, University Hospital Zurich, CH-8091 Zurich, Switzerland.*
E-mail: spyros.kollias@usz.ch

a *D. I. Hollnagel, S. S. Kollias*
Institute of Neuroradiology, University Hospital Zurich, Zurich, Switzerland

b *D. I. Hollnagel, D. Poulikakos*
Laboratory of Thermodynamics in Emerging Technologies, Department of Mechanical and Process Engineering, ETH Zurich, Zurich, Switzerland

c *P. E. Summers*
Department of Neurophysiology, University of Modena and Reggio Emilia, Modena, Italy

d *P. E. Summers*
Department of Neuroradiology, John Radcliffe Hospital, University of Oxford, Oxford, UK

Contract/grant sponsor: Swiss National Science Foundation (SNF); contract/grant number: 3200B0-100355.

Abbreviations used: *CFD, computational fluid dynamics; CT, computer tomography; DSA, digital subtraction angiography; DICOM, digital imaging and communications in medicine; IGES, initial graphics exchange specification; LDV, laser Doppler velocimetry; MVD, mean velocity difference; NURBS, non-uniform rational B-spline; PC-MRA, phase-contrast magnetic resonance angiography; PVD, peak velocity difference; R, correlation coefficient; RMSE, root mean squared error; ROI, region of interest; SNR, signal-to-noise ratio; VENC, velocity encoding; VRML, virtual reality modeling language.*

To address the need for improved spatial resolution (12–14), and to overcome the ensuing loss in signal to noise, we have obtained quantitative 3D PC-MRA velocity maps in a 3 T MR scanner. This allowed the slice thickness to be reduced, while yielding SNRs greater than that of a single average 2D PC-MRA velocity mapping study at 1.5 T, through the greater polarization effect of higher magnetic field, and the averaging effect of 3D acquisition. We have previously shown that velocity measurements obtained by 3D PC-MRA velocity mapping are in good agreement with laser Doppler velocimetry (LDV) measurements for steady flow in a realistic (in geometry and size) arterial aneurysm model under certain conditions (15).

For describing the hemodynamic effects of the flow within an aneurysm, apart from the velocity field itself, other properties such as the wall shear stresses and pressure also constitute very important clinical information. At present, it is impossible to measure these characteristics non-invasively. Two possibilities exist for obtaining these descriptors of the hemodynamic forces in a specific arterial segment of an individual patient based on non-invasive measurements: either deriving them directly from the measured velocity field (16–18), or to use the velocity field measurements as patient-specific inlet and outlet conditions in a numerical simulation (CFD) of the flow field and derive the flow characteristics from this field (19–24). In either approach, the quality of the derived parameters relies on the accuracy of the PC-MRA as a source of the velocity field data. The sensitivity of the two approaches to imperfections in the PC-MRA data is likely to be different, and each must be validated against an independent method. To achieve this goal, in the present work, the transient velocity field was measured in a well-defined realistic silicone phantom with 3D PC-MRA and with an alternative spatially and temporally resolved velocimetry technique, LDV. Subsequently, both measurements were compared to each other and to the velocities obtained through numerical simulations.

To our knowledge, direct comparison of both, PC-MRA and CFD with a reference method (LDV) in the same model of a small realistic artery setting has not been reported so far.

EXPERIMENTAL

Model and setup

The measurements and numerical simulations were performed in a realistic intracranial aneurysm model with transient flow. The preparation and construction of the silicone model for the LDV and PC-MRA measurements has been described in detail in Reference (15). The inlet of the model is the temporal segment of the internal carotid artery at the skull base and has a diameter of 3.7–4 mm. A saccular aneurysm is located at the origin of the posterior communicating artery. The posterior communicating artery and the posterior cerebral artery are included in the model, as are the bifurcation of the internal carotid artery distal to the aneurysm and the ensuing anterior cerebral and middle cerebral arteries. The very small ophthalmic artery is not included in the model. The outlets of the model are therefore the anterior, middle, and posterior cerebral arteries (Fig. 1a).

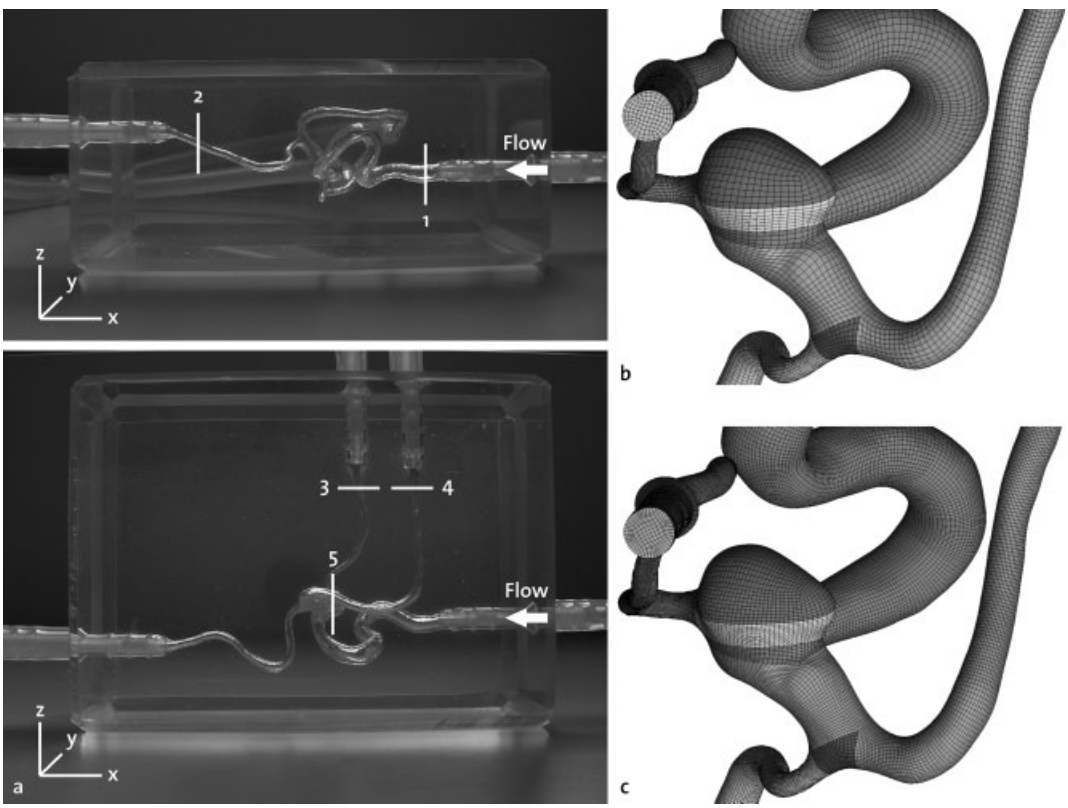

Figure 1. Model. (a) Silicone model and measurement positions within the model. Two measurements (internal cerebral artery (1) and anterior cerebral artery (2)) were performed with the model laying flat and three measurements (posterior cerebral artery (3), middle cerebral artery (4) and aneurysm (5)) were performed with the model in vertical position due to the limited accessibility of the flow regions using the laser. Therefore, the coordinate system changes relative to the model. (b) Coarse mesh with 185,170 hexahedral cells over the entire geometry. The size of the cells is between $2.86 \times 10\text{-}4$ mm^3 and $1.09 \times 10\text{-}2$ mm^3. (c) Fine mesh with 851,330 hexahedral cells over the entire geometry. The size of the cells is between $7.43 \times 10\text{-}5$ mm^3 and $2.38 \times 10\text{-}3$ mm^3.

NMR IN BIOMEDICINE

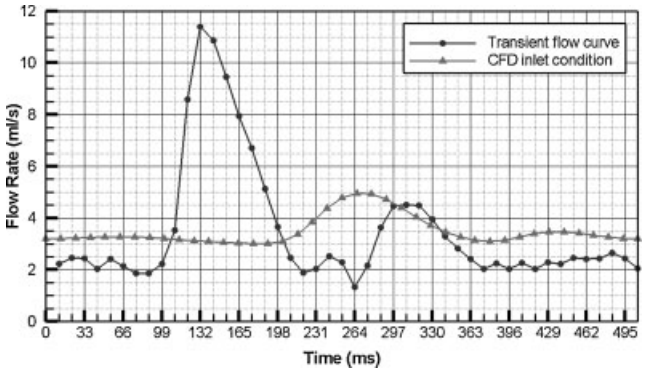

Figure 2. Applied flow curves. The dark curve with the circles is applied by the computer controlled pump. The gray curve with the triangles is applied in the numerical simulations. These curves differ due to the damping caused by the long elastic tube leading to the model, which causes the flow reaching the silicone model to change. Therefore, the transient mass flow curve was calculated from the LDV velocities measured at the internal carotid artery position (1) and is then applied as a bulk mass flow to the extended inlet of the virtual model. While passing through the extension the flow develops thus resulting in comparable velocity conditions at all measurement positions and for all measurement methods.

The blood mimicking fluid used for the measurements consisted of a mixture of 59.4% by weight of glycerol in water with hollow glass spheres (Ø 10 μm) added as seeding particles for the LDV. The fluid had the same refraction index ($n = 1.412$) as the silicone model to minimize the errors due to refraction in the LDV measurements. The T1 and T2 values of the fluid were 500 and 45 ms, respectively. Its density was 1151.5 kg/m^3 and viscosity 10.3 mPa · s. The density of blood is 1048 kg/m^3 (25) and for an assumed constant viscosity under the specific flow condition of 4 mPa · s (26–28), the flow was adjusted to *in vivo* blood properties by matching the Reynolds and Womersley numbers. An *in vivo* pulse rate of 60 per minute was assumed and the resulting frequency from the Womersley number was 2 Hz. The peak flow for the pulsating flow was 11.4 mL/s and the average flow was 3.494 mL/s. These values correspond to observations from the literature (29–33). To maintain an accurate and reproducible flow through the model, a computer controlled pump suitable for MR environments (CompuFlow 1000 MR, Shelley Medical Imaging Technologies, Mississauga, Canada) was used for generating transient flow curves with less than 1% variance (34,35). A pre-installed carotid artery flow curve was used after adjustment to the above-mentioned values (Fig. 2). The vascular model was connected to the pump system via 6 mm diameter silicone tubes. A fluid showing the same parameters was modeled in the Ansys CFX simulation software. Due to the damping caused by the long elastic tubing leading to the model, the flow curve that actually reached the model had changed. Therefore, the flow curve applied in the numerical simulation had to be adjusted. This was done by calculating the mass flow from the LDV measured values at the internal carotid artery (measurement position 1) and applying this mass flow as inlet condition in the virtual model (Fig. 3).

Velocity investigations

The velocity field in the model was investigated by using the following tools: (a) an LDV system (Dantec, Skovlunde, Denmark), (b) a retrospectively gated 3D PC-MRA sequence obtained in an Achieva 3 T MR scanner (Philips Medical Systems, Best, The Netherlands) using an 8-channel head coil, and (c) computational fluid dynamics (CFD) using CFX (Ansys Europe, Inc.) (Fig. 3). Considering the impracticality of performing LDV throughout the

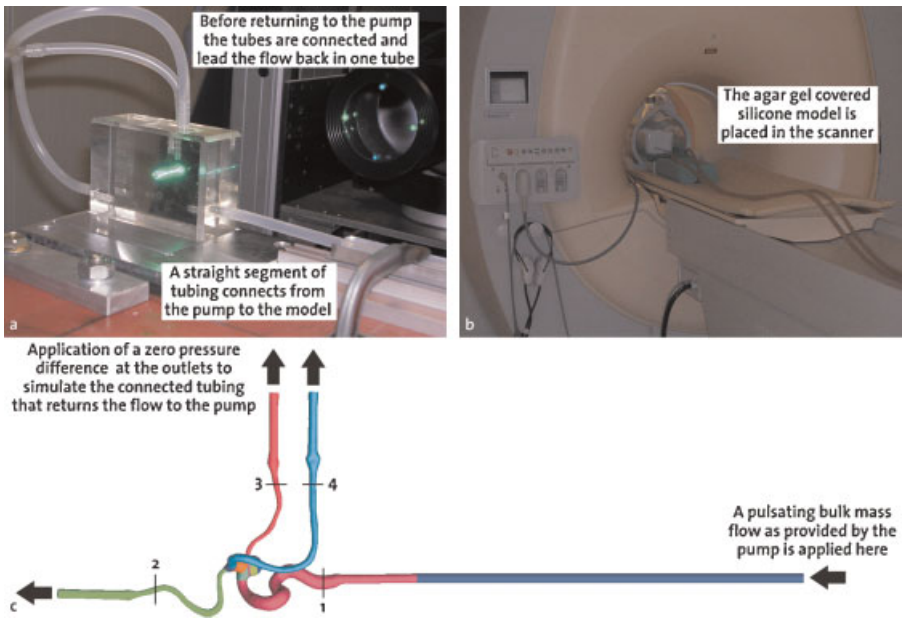

Figure 3. Illustration of the experimental setup. (a) Laser Doppler velocimetry: four laser beams (two green for the horizontal and two blue for the vertical velocity measurements) intersect in the flow region of the silicone model. The tube leading to the model is fixed rectilinear for more than 24 cm (40 × tube diameter) to ensure that the flow entering the model is fully developed. The outlet tubes are converging before returning to the pump. (b) This same silicone model setup, covered with agar gel, was placed in the MR scanner to achieve similar conditions for the phase-contrast MRA velocity mapping. Also here, the tube leads straight to the model and the outlet tubes were connected. (c) Virtual model: the proximal portion was extended (dark blue) to allow the application of a bulk mass flow and still assure a fully developed flow at the level of the "internal carotid artery" (measurement position 1). The connection of the outlets was simulated by applying a zero pressure difference between them.

entire model, comparisons are limited to five cross-sectional locations in the model, which are indicated in Figs 1a and 3.

The measurement planes were perpendicular to the flow direction for the relatively straight artery segments at the internal carotid artery (measurement position 1) and the middle cerebral artery (measurement position 4). Thus, very low in-plane velocities are expected at these positions. However, at the anterior and posterior cerebral arteries (measurement positions 2 and 3), the curvature of the vessels resulted in the imaging planes intersecting the flow at significant angles during the cross-sectional measurements (22° in the *xz*-plane and 18° in the *xy*-plane for the anterior cerebral artery and 9° in the *xz*-plane for the posterior cerebral artery), which may lead to in-plane velocity components. At the average flow velocity, the length of the tubing on the straight path from the opening of the scanner bore to the phantom provided 5.4 s (equal to 10.8 × T1 of the fluid) of exposure to the magnetic field, sufficient to provide full polarization for all spins assuming fully developed flow. In CFD, the flow was simulated in the entire geometry under the same conditions as the PC-MRA and LDV measurements. For the comparative analysis, the same planes as in the measurements were extracted from the calculated flow field.

LDV measurements

LDV is a non-contact optical measurement method to obtain velocity components in fluids (36). The principle of the LDV is the Doppler effect: the laser acts as a non-moving transmitter and particles in the fluid (added glass spheres, Ø 10 μm) act first as moving receivers and then as moving transmitters of the reflected light being detected by a non-moving receiver. The detected light is frequency-shifted relative to that sent from the laser, allowing the velocity of the reflecting particle to be calculated. In practice, this frequency shift is too small to be detected. Instead, a two laser-beam set up is used, allowing the velocity component of the reflecting particle in the plane of the beams and perpendicular to the line bisecting the angle between the beams to be calculated (36,37). For our measurements, two argon-ion lasers with wavelengths of 514.5 nm (green) and 488 nm (blue) were used to simultaneously record the two velocity components.

Velocity distributions (arising from a sensitive ellipsoidal volume of approximately 2.5×10^{-3} mm^3) were measured at points along radial lines passing through the maximum velocity in each cross-section. The spacing of the points varied between 0.05 and 0.15 mm and 200 000 signals were recorded per point. For each point, separate distributions of the measured velocities were formed for 40 time intervals on the basis of binning the arrival time of the measured signal relative to the pump trigger signal. This resulted in about 5000 signals per interval. Within each of these intervals the mean value was taken to be the velocity at this specific point and interval of time. Each measurement of a temporal velocity profile at a spatial point required 150–700 s, depending on the rate of scatter detection.

PC-MRA measurements

A standard 3D PC-MRA sequence was used with parameters optimized to provide the maximum spatial resolution within a reasonable acquisition time. For the artery regions the imaging volume consisted of 15 slices with a thickness of 1 mm each at the internal carotid, posterior, and middle cerebral arteries and 0.7 mm at the anterior cerebral artery, while 19 slices with a thickness of 0.7 mm each were obtained when imaging the aneurysm in order to improve the signal to noise ratio (SNR). The middle slice of the volume was placed at the cross-sectional plane of interest and is the only slice to undergo analysis. The additional slices allow, compared to a 2D slice, a lower acquisition bandwidth of 618.7 Hz for the minimum available echo time (TE) of 4.2–5.5 ms, while also imparting an averaging benefit for SNR improvement. The repetition time (TR) was chosen to be 25 ms and the flip angle 8°. The matrix contained 320 × 224 pixels in a field of view (FOV) of 250 × 105 mm. The velocity encoding (VENC) was set to slightly exceed the maximum expected velocity, in order to maximize the velocity to noise ratio (VNR). Correspondingly, the VENC used when measuring in-plane components was lower than that used when acquiring the through-plane component. Signal averaging (NSA, NEX, ACQ) was used for the anterior, middle, and posterior arteries (NSA = 2) and for the aneurysm (NSA = 3). Retrospective triggering with bilinear interpolation was used to generate a total of 40 temporally resolved velocity maps for each of the 15 slices in the 3D PC-MRA volume for a spatial resolution of 0.469 mm in a 14–30 min scan time. The MR velocity data were exported from the scanner in DICOM format and the 40 time instant files from the central slice of each 3D PC-MRA dataset were used for comparison with LDV and CFD.

To minimize the Maxwell terms in the background due to eddy currents, all measurements were performed within 2 cm of the isocenter without the manufacturer's background correction. The mean and standard deviation of differences from zero in ROIs defined in the surrounding static gel were less than 1.5 and 3.5% of the VENC, respectively. As these ROIs were farther from the isocenter than the vessels, they can be expected to overestimate the severity of the errors at the vessel sites. Therefore no further steps were taken to correct the background.

Numerical simulations

For the virtual geometry, the silicone model was measured with high resolution CT scans ($0.2 \times 0.2 \times 1$ mm^3) in two spatial directions and segmented manually using the Amira software (Mercury Computer Systems, Bordeaux, France). The images were transferred to Geomagic Studio (Geomagic, Research Triangle Park, North Carolina, USA) as virtual reality modeling language (VRML) files. In Geomagic Studio they were merged, patched and rendered into a non-uniform rational B-spline (NURBS) surface. This was transferred into the Ansys ICEM-CFD grid generation software (Ansys Inc., Canonsburg, PA, USA) as an initial graphics exchange specification (IGES) file. With ICEM-CFD, the inlet was extended with a straight tube to enable virtual application of a pulsating bulk mass flow as the inlet condition and also allow the flow to develop until it reaches the modeled arteries. Three block structured hexahedral meshes with 385 blocks and 185 170 (coarse), 407 429 (medium), and 851 330 (fine) hexahedrons were generated for this geometry (Fig. 1b,c).

The velocity field in this model was calculated using the Ansys CFX 11 software with a transient mass flow curve as the inlet condition as shown in Fig. 2. A multigrid method was used and the order of residuals decreased by more than four orders of magnitude to 10^{-8}. The simulations were run on three different sized grids as described above for four periods with three time step sizes ($t_1 = T/80 = 6.325 \times 10^{-3}$ s, $t_2 = T/160 = 3.1625 \times 10^{-3}$ s, and $t_3 = T/200 = 2.53 \times 10^{-3}$ s, with $T = 0.506$ s being the time of one

NMR IN BIOMEDICINE

Table 1. Simulation times and numbers of processors used on the three grids for the different time step sizes

	Coarse (185 170 hexahedrons)		
Time step size (s)	6.325×10^{-3}	3.1625×10^{-3}	2.53×10^{-3}
Processors	12	16	20
Total CPU time (s)	257 150	463 490	532 890
Total wall clock Time (s)	31 320	44 610	47 910
	Medium (407 429 hexahedrons)		
Time step size (s)	6.325×10^{-3}	3.1625×10^{-3}	2.53×10^{-3}
Processors	16	16	20
Total CPU time	533 040	958 210	1 177 410
Total wall clock Time (s)	50 340	82 530	84 440
	Fine (851 330 hexahedrons)		
Time step size (s)	6.325×10^{-3}	3.1625×10^{-3}	2.53×10^{-3}
Processors	16	16	20
Total CPU time	1 035 130	1 841 980	2 255 600
Total wall clock Time (s)	89 840	112 300	113 000

period) on up to 20 processors. The CPU times were between 257 150 s and 2 255 600 s, which resulted in total wall clock times between 31 320 s and 113 000 s (Table 1).

Independence studies showed that the different grids, time step sizes, and periods give similar results and therefore are valid. The differences between the time step sizes and periods were less than 1% and the differences on critical positions, like within the aneurysm, were less than 5%. Therefore, the results of the fine grid simulations were assumed to be correct and were further used for comparisons with the measurements.

Analysis

Prior to comparison of the measurement and simulation data, cubic interpolation was used to fit surfaces to the acquired velocities in each cross-section of interest (Matlab, Version 7.0.1.24704 (R14) Service Pack 1, The MathWorks, Inc., Natick, MA, USA). The velocity component maps were qualitatively compared at two specific instants of the pump cycle (190 ms, just before the increase of the flow, and 266 ms, at the peak flow) using surface plots, contour lines, and profiles along cardinal directions in each cross-section. The interpolated velocity components were individually subjected to correlation analysis between the measurements and simulation for the cross-sections at specific time instants as a whole. The main flow direction describes the through-plane velocity component and the secondary flow direction describes one in-plane velocity component. The instantaneous mean velocities for the through-plane flow direction in each modality were calculated, plotted over time, and the correlation coefficient between the two curves determined. The two time instants examined are indicated in the respective figures relative to these curves.

To quantitatively compare the different methods, we made use of several characteristic numbers calculated for each cross-sectional location, velocity direction, and time instant. The results were then plotted over time. The characteristic numbers are the following:

- correlation coefficient *(R)*, ideal $R = 1$;
- root mean squared error relative to maximum LDV velocity (RMSE), ideal RMSE = 0;
- coefficients (*m, b*), the slope and intercept of the normalized regression line: $\mathrm{PCMRA}' = m \cdot \mathrm{LDV}' + b$, ideal $m = 1$, ideal $b = 0$ (with $\mathrm{PCMRA}' = \mathrm{PCMRA}/\mathrm{LDV}_{max}$ and $\mathrm{LDV}' = \mathrm{LDV}/\mathrm{LDV}_{max}$).

For the through-plane velocity direction some more characteristic numbers are included:

- peak velocity difference relative to maximum LDV velocity (PVD), ideal PVD = 0;
- mean velocity difference relative to mean LDV velocity (MVD), ideal MVD = 0;
- correlation coefficients of the mean and peak flow curves.

For each anatomical location and velocity direction, the means of the characteristic numbers are determined. Taking the LDV measurements as the standard for reference, we consider differences from these measurements to represent errors in the CFD or PC-MRA values. The errors (*E*) of the characteristic numbers related to the maximum or mean velocities, respectively, are rated as follows: $E \leq 5\%$: *very good* (++), $5\% < E \leq 10\%$: *good* (+), $10\% < E \leq 15\%$: *weak* (−), $E > 15\%$: *poor* (−−).

RESULTS

Internal carotid and middle cerebral artery

The measurement planes at the internal carotid artery (measurement position 1) and the middle cerebral artery (measurement position 4) were perpendicular to the flow axis and resulted in high through-plane and small in-plane velocities. The through-plane velocities at the internal carotid artery are shown in Figs 4–7. The contour plots (Fig. 4a) were qualitatively similar and showed the same patterns at all times, with backflow regions being reproducible with all three methods. Slight differences occurred near the boundaries and the noise in the PC-MRA data could be observed. From the contour plots, it was obvious that CFD and LDV velocity patterns were in better agreement with each other than with PC-MRA. The CFD simulation calculated a lower peak velocity than measured with LDV and PC-MRA for the internal carotid artery (Fig. 5), but slightly overestimated the velocities for the middle cerebral artery. The mean and peak velocity curves were in very good agreement, with very high

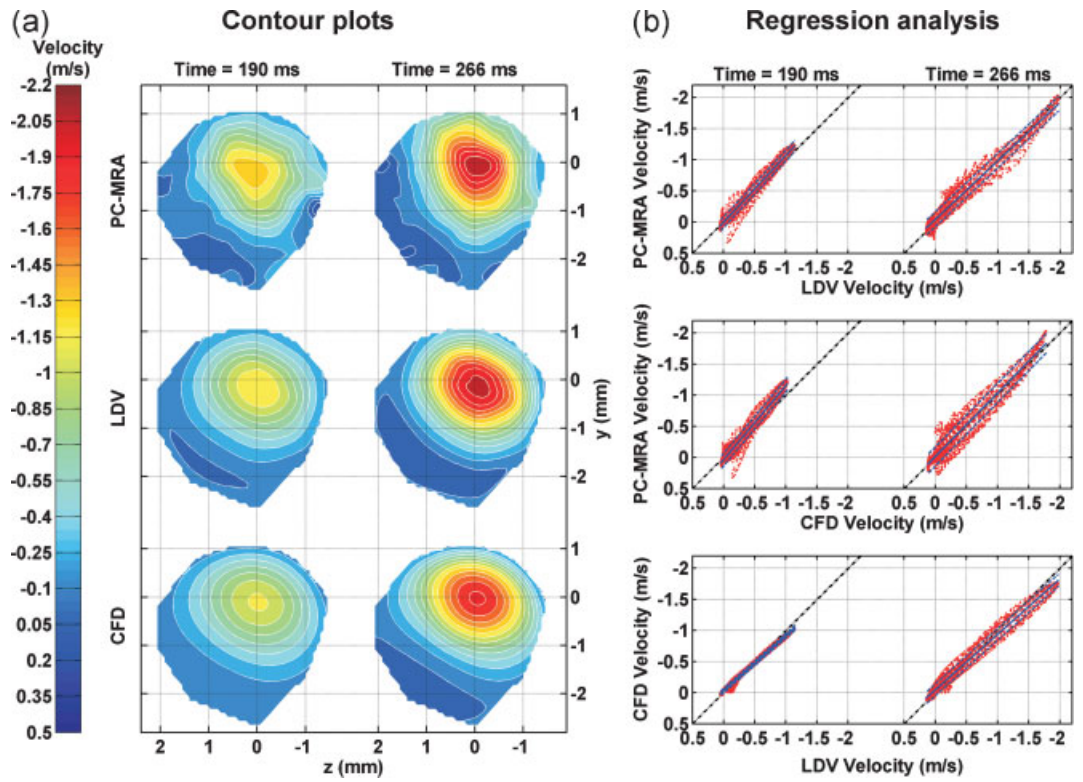

Figure 4. (a) Through-plane velocities at the internal carotid artery demonstrate similar patterns in the contour plots. Note also slightly lower values in the CFD and noise in the PC-MRA plots. (b) The regression analysis shows low dispersion and regression lines very close to identity.

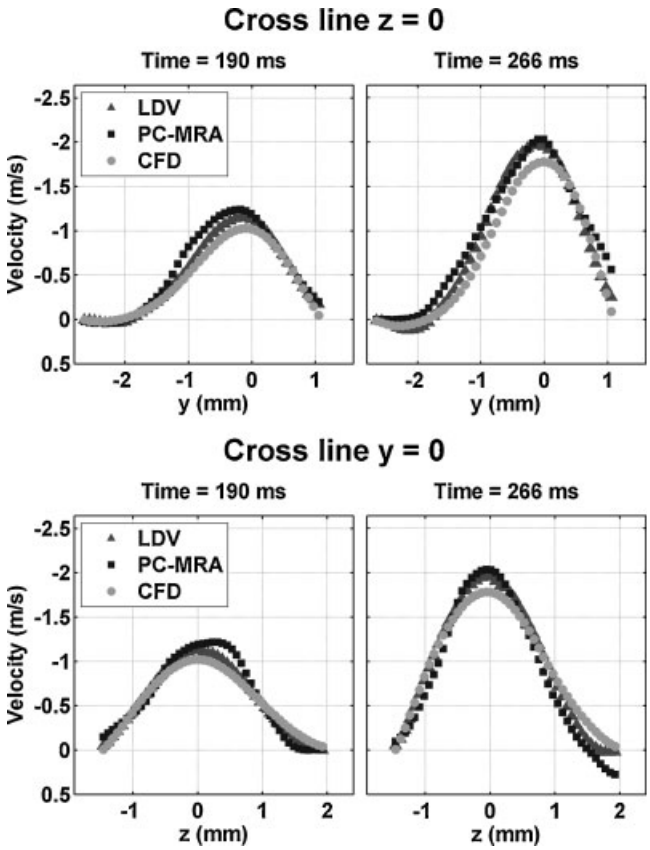

Figure 5. The profile lines of the through-plane velocities at the internal carotid artery show good agreement between the methods, except for slight differences at the peak.

correlation coefficients, but with some absolute differences (Fig. 6), especially around the time of peak flow for the middle cerebral artery. This was reflected in the regression analysis (Fig. 4b) which, despite showing high correlation coefficients (R) throughout the whole cycle (Fig. 7), revealed a tendency for lower CFD velocities, where the PC-MRA *versus* LDV regression lines were close to identity at the internal carotid artery (Fig. 4b). The variance per time instant was highest for the low velocities at the boundaries. The RMSEs in all method comparisons are of the same order and show errors of less than 10% for the internal carotid artery and for the middle cerebral artery, being especially low between CFD and LDV at time instants other than peak flow (Table 2).

In the analysis of the in-plane velocity components for the internal carotid artery and middle cerebral artery the contour plots also showed good qualitative agreement despite the very low absolute velocities. The velocities obtained with CFD are strongly underestimated at the internal carotid artery, although the patterns are similar. At the middle cerebral artery, the contours of the CFD and LDV data were very similar, while the PC-MRA data did not reproduce the specific flow patterns. Notably however, the in-plane velocities observed here were very low, at about 5% of the maximum through-plane velocity. The correlation between the methods was very high for all time points, except for the comparisons against CFD at the internal carotid artery (Table 2). The regression plots showed low dispersion of the measurements, which was again highest at velocities near zero and resulted in mean RMSEs that were consistent over the whole cycle. The slope of the regression lines for lower mean velocities was closer to unity than for velocities at the time of peak flow. For the comparisons against CFD at the internal carotid artery, the regression lines were offset and rotated, because of the very low CFD velocities.

NMR IN BIOMEDICINE

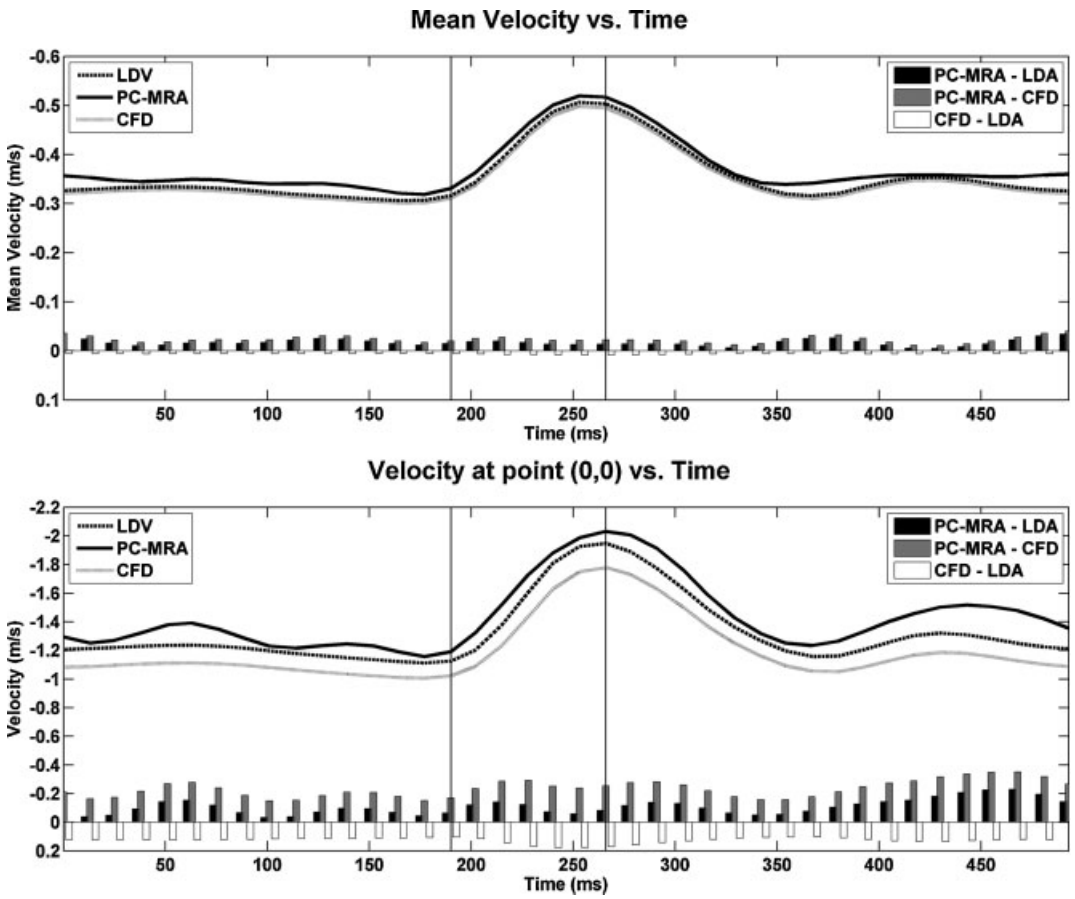

Figure 6. Mean through-plane velocities (above) and through-plane velocities at the point of maximum velocity (below) at the internal carotid artery are plotted against time. The differences between the curves are shown as bar plot. The comparisons of the curves show very high correlation coefficients (Table 1).

Anterior and posterior cerebral arteries

The measurement planes at the anterior (measurement position 2) and posterior (measurement position 3) cerebral arteries were not perpendicular to the flow axis and resulted in through-plane and in-plane velocities of the same order (Figs 8 and 10). For the through-plane velocity measurements the methods gave generally comparable impressions of the velocities, but differed substantially in the detailed flow patterns (Fig. 8a). Similarities were greatest between CFD and LDV while rather weak

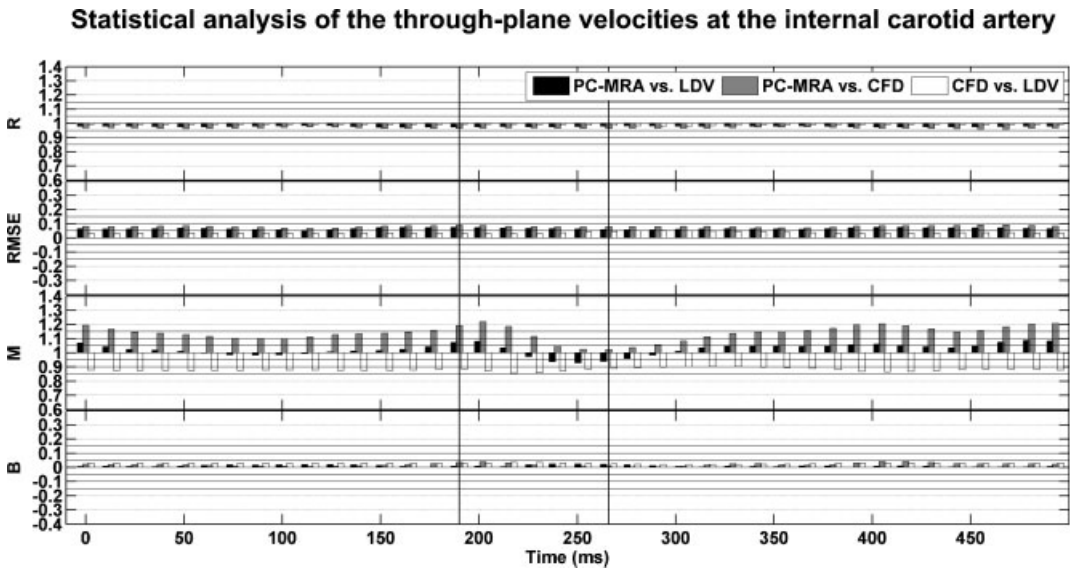

Figure 7. The results between the methods are plotted over time. The plot shows very low errors for the correlation coefficient (R), the root mean squared error (RMSE) and the intercept of the regression line (B). The slope of the regression line (M) shows slightly larger errors for comparisons with CFD.

Table 2. Comparative results of the three different measurement methods in the arteries. Percentage differences from the ideal value and rating as described in the Section 'Analysis'

	Internal cerebral artery						Anterior cerebral artery					
	PC-MRA–LDV		PC-MRA–CFD		CFD–LDV		PC-MRA–LDV		PC-MRA–CFD		CFD–LDV	
	%	Rating	%	Rating	%	Rating	%	Rating	%	Rating	%	Rating
						Through-plane						
R	2.21	+ +	3.34	+ +	0.97	+ +	17.08	− −	21.19	− −	8.62	+
RMSE	−6.55	+	−8.02	+	−3.66	+ +	−9.34	+	−10.35	−	−9.28	+
m	2.37	+ +	13.78	−	11.91	−	32.07	− −	41.13	− −	0.29	+ +
b	0.68	+ +	−1.83	+ +	2.69	+ +	16.54	− −	37.53	− −	−24.93	− −
PVD	5.74	+	17.53	− −	−11.79	−	−20.63	− −	−2.54	+ +	−18.09	− −
MVD	4.94	+ +	6.68	+	−1.74	+ +	−8.57	+	26.35	− −	−34.92	− −
R_{MFC}	0.71	+ +	0.72	+ +	0	+ +	8.39	+	8.55	+	1.95	+ +
R_{PFC}	2.31	+ +	2.61	+ +	0.1	+ +	10.01	−	10.89	−	1.13	+ +
Average		+ 1.75		+ 0.875		+ 1.25		− 0.75		− 0.875		+ 0.25
						In-plane						
R	4.68	+ +	22.9	− −	23.62	− −	18.36	− −	14.32	−	9.28	+
RMSE	−8.49	+	−18.02	− −	−6.29	+	−8.06	+	−7.15	+	−11.63	−
m	18.72	− −	124.78	− −	77.65	− −	54.15	− −	56.08	− −	0.31	+ +
b	10.8	−	16.86	− −	−0.24	+ +	31.82	− −	38.52	− −	−12.11	−
Average		0		−2		−0.25		−1.25		−1		+ 0.25
						Through-plane and in-plane						
Average		+ 1.167		−0.833		+ 0.75		−0.917		−0.917		+ 0.25

	Posterior cerebral artery						Middle cerebral artery					
	PC-MRA–LDV		PC-MRA–CFD		CFD–LDV		PC-MRA–LDV		PC-MRA–CFD		CFD–LDV	
	%	Rating	%	Rating	%	Rating	%	Rating	%	Rating	%	Rating
						Through-plane						
R	21.37	− −	9.34	+	5.92	+	10.55	−	8.15	+	2.83	+ +
RMSE	−11.84	−	−7.91	+	−8.65	+	−9.33	+	−8.22	+	−7.61	+
M	33.23	− −	31.8	− −	6.45	+	25.23	− −	40	− −	24.54	− −
B	13.79	−	25.49	− −	−22.14	− −	9.05	+	15.95	− −	−11.45	−
PVD	−12.2	−	−0.69	+ +	−11.51	−	−0.4	+ +	−12.52	−	12.12	−
MVD	−9.57	+	21.8	− −	−31.37	− −	−8.09	+	−10.93	−	2.84	+ +
R_{MFC}	9.51	+	9.56	+	0.44	+ +	2.61	+ +	3.83	+ +	0.73	+ +
R_{PFC}	6.74	+	7.04	+	0.63	+ +	1.42	+ +	2.8	+ +	0.92	+ +
Average		−0.5		0		+ 0.25		+ 0.75		0		+ 0.625
						In-plane						
R	38.34	− −	35.2	− −	7.83	+	7.03	+	7.27	+	2.64	+ +
RMSE	−32.3	− −	−31.24	− −	−14.8	−	9.76	+	9.95	+	8.1	+
m	40.91	− −	30.28	− −	17.45	− −	9.2	+	30.54	− −	27.01	− −
b	−6.93	+	−4.21	+ +	−3.62	+ +	−7.68	+	12.94	−	−27.85	− −
Average		−1.25		−1		0		+ 1		−0.25		−0.25
						Through-plane and in-plane						
Average		−0.75		−0.33		+ 0.167		+ 0.83		−0.083		+ 0.33

R_{PFC}, correlation coefficient of the peak velocity curves; R_{MFC}, correlation coefficient of the mean flow curves.

correlation coefficients were obtained for the comparisons with PC-MRA (Table 2). The CFD simulations underestimated the velocities (Fig. 9), and the regression analysis showed that the differences between the velocities were larger than for the internal carotid artery (Fig. 8b). The variations between the techniques were greatest at lower velocities (i.e. at the boundary of the flow region) throughout the pump cycle and lower for faster flow regions. The cross-line plots showed the same patterns for CFD and LDV as opposed to the PC-MRA. The profile lines also showed that the PC-MRA measurements underestimated the peak velocity at the posterior cerebral artery, and the CFD simulations showed slightly reduced values at the

NMR IN BIOMEDICINE

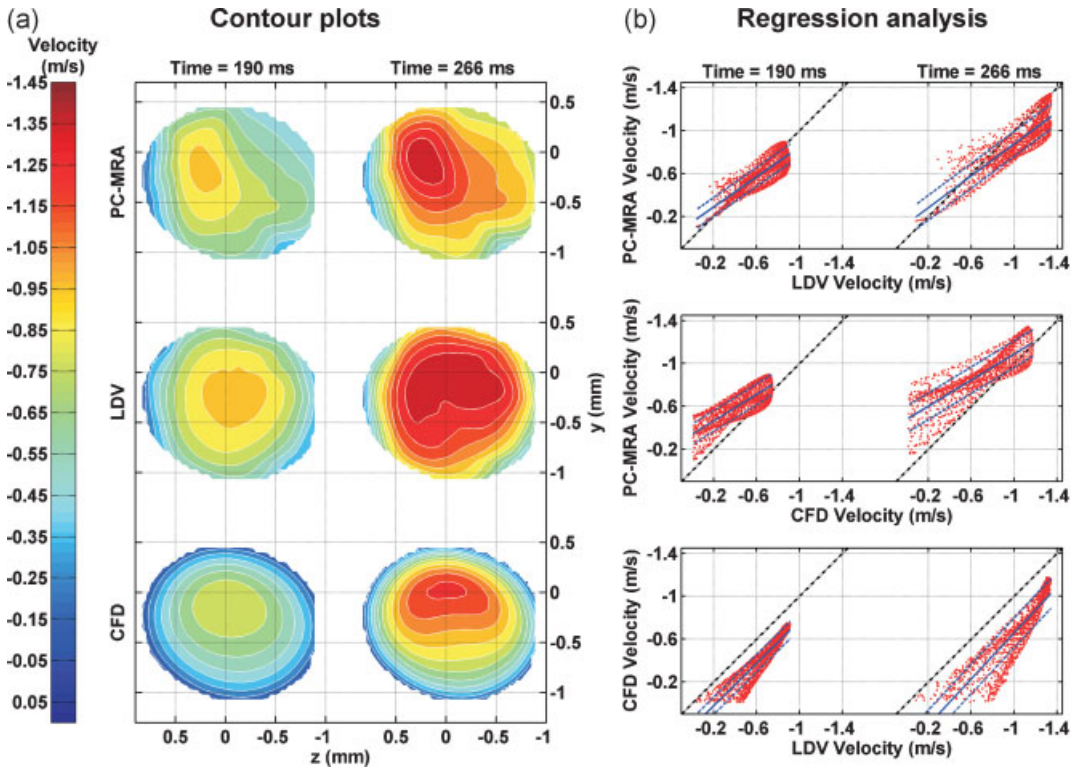

Figure 8. (a) Through-plane velocities at the anterior cerebral artery demonstrate contour plots with similar patterns, though finer flow features are not reproduced with PC-MRA. (b) The regression analysis shows higher dispersion of velocities than in the internal carotid artery, with the slopes and intercepts of the regression lines varying over the cycle.

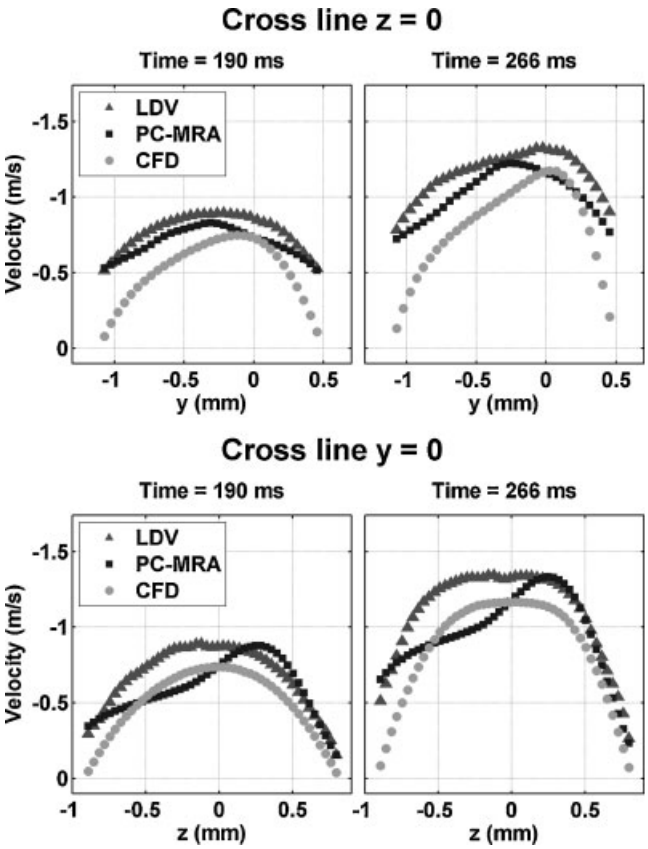

Figure 9. The profile lines of the through-plane velocities at the anterior cerebral artery show similar patterns, except in the peak flow region.

other time instants. In the plots of the characteristic numbers for the comparisons with PC-MRA, the differences between the characteristic numbers and their ideal values were seen to be consistently around or greater than 10%, while those between CFD and LDA were less than 10%, except for the regression line intercept, which shows errors of more than 20%. The slopes of the normalized regression lines were reduced more than 30% below unity in the PC-MRA comparisons, whereas these errors average below 10% for the CFD–LDV comparison (Table 2). The velocity curves were highly correlated for the CFD–LDA comparison, despite the underestimation of the absolute values by the CFD simulation. The peak velocity curve for the anterior cerebral artery was similar for the CFD and PC-MRA measurements, while for the LDV measurements it was higher. The peak velocity curve for the posterior cerebral artery was very close for the CFD and LDV and lower for the PC-MRA (Table 2).

The flow patterns of the in-plane velocity components from the LDV and CFD were very similar (Fig. 10a) also for the reversed flow regions at the posterior cerebral artery, while the PC-MRA patterns showed distinct differences. These observations were supported by the cross-line plots, which demonstrate that the CFD and LDV data overlaid each other but the PC-MRA showed rather dissimilar patterns (Fig. 11). While the absolute values matched very well between LDV and CFD, the PC-MRA velocities were notably lower, most prominently around the time instant of the through-plane peak flow. The observed differences were clarified in the regression analysis (Fig. 10b). The scatter plots showed a rather low dispersion and regression lines close to unity for the CFD–LDV comparisons and RMSEs of around 10%, but in the comparisons with PC-MRA, both the slope and the intercept showed high errors (Table 2).

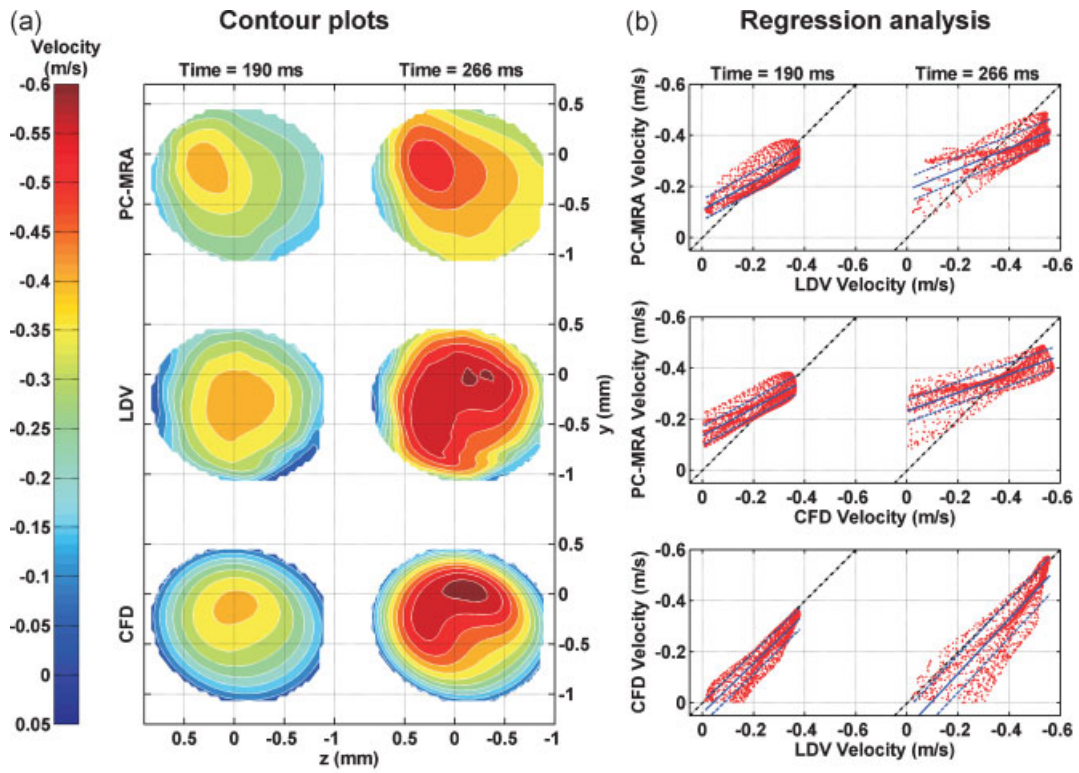

Figure 10. (a) The contours of the in-plane velocities at the anterior cerebral artery demonstrate that PC-MRA underestimates and poorly reproduces the flow patterns. (b) The regression analysis shows that slope and intercept differ significantly from unity for comparisons with PC-MRA.

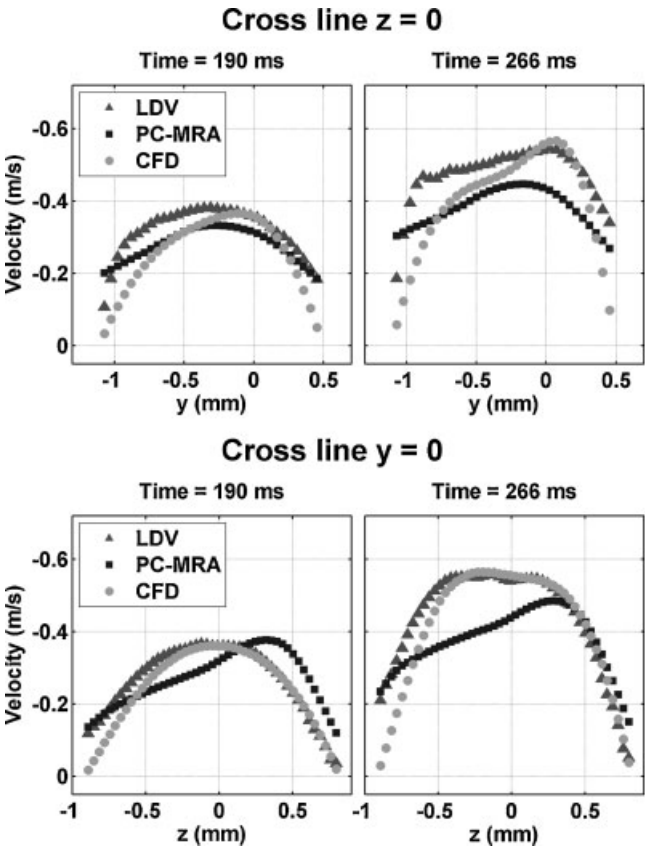

Figure 11. (a) The profile lines of the in-plane velocities at the anterior cerebral artery indicate clear differences in the flow patterns in comparison with PC-MRA.

Aneurysm

Measurements within the aneurysm (measurement position 5) with LDV were only performed along two lines and therefore no surface could be fitted. A comparison was made with the corresponding lines in the slices from the PC-MRA and CFD data. The contour plots with the LDV lines and the profile lines are shown in Figs 12 and 13 for the through-plane and in-plane velocities, respectively. They showed pronounced differences that were also reflected in the extremely high differences of the characteristic parameters (Table 3). The same tendencies in the velocity patterns can be observed, but the characteristic numbers always show errors of over 15% in comparison with the PC-MRA measured data.

DISCUSSION

An important question for the preparation of patient-specific velocity field analyses is to establish whether non-invasive PC-MRA measurements alone, or combined with CFD modeling can be reliably used for determining the likely hemodynamic risk factors for aneurysm growth, including shear stress, pressure, and residence time. The specifics of the cross-sectional velocity profiles are important for the calculation of these secondary parameters and the spatially resolved accuracy of the velocity field must be adequate to support the calculations.

The spatial resolution available with CFD and LDV offers a distinct advantage over PC-MRA for depicting the dynamics of the flow. In the present study, we have used interpolation from the acquisition resolution of the PC-MRA to match that of LDV. To avoid artifacts in the interpolation, it is necessary that the velocity

NMR IN BIOMEDICINE

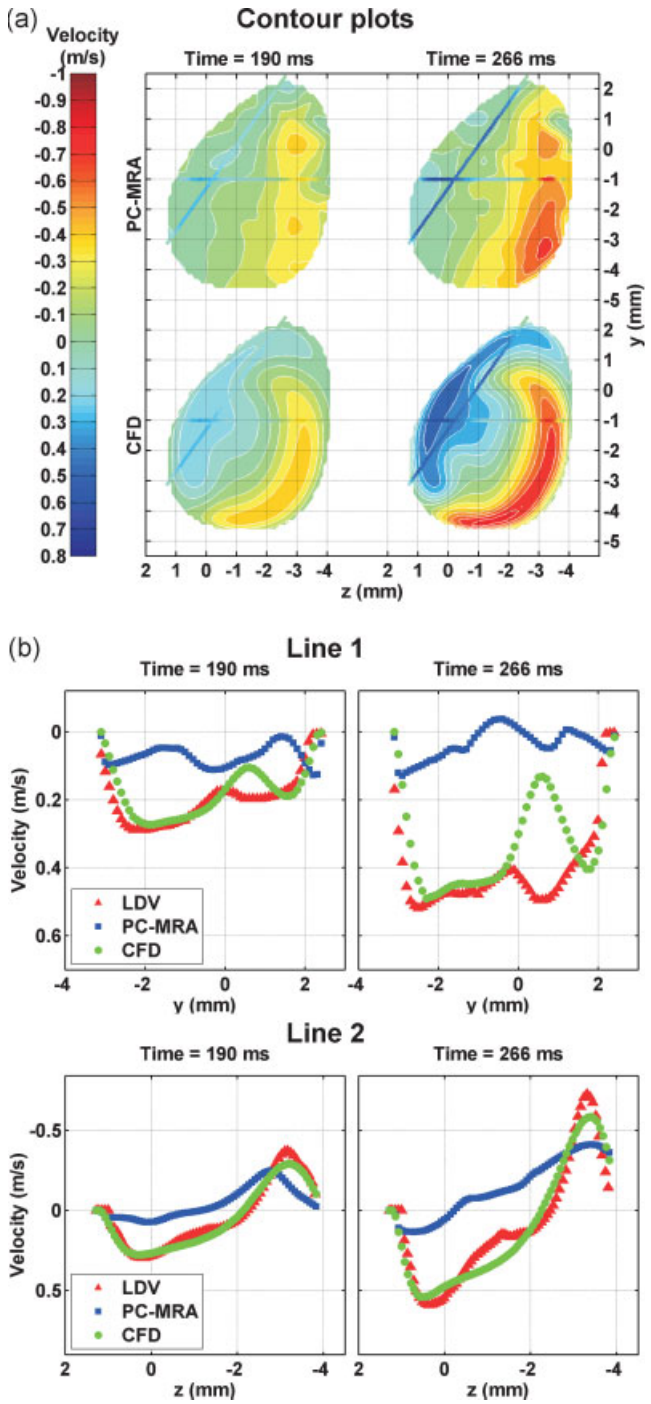

Figure 12. The contour plots (a) of the through-plane velocities in the aneurysm show the PC-MRA and CFD data in the entire cross-section and the lines measured with LDV. In the line plots (b) the extracted data from the PC-MRA and CFD are shown with the lines measured with LDV. It is demonstrated that the LDV and CFD velocity values and patterns are similar, while the PC-MRA data differ significantly.

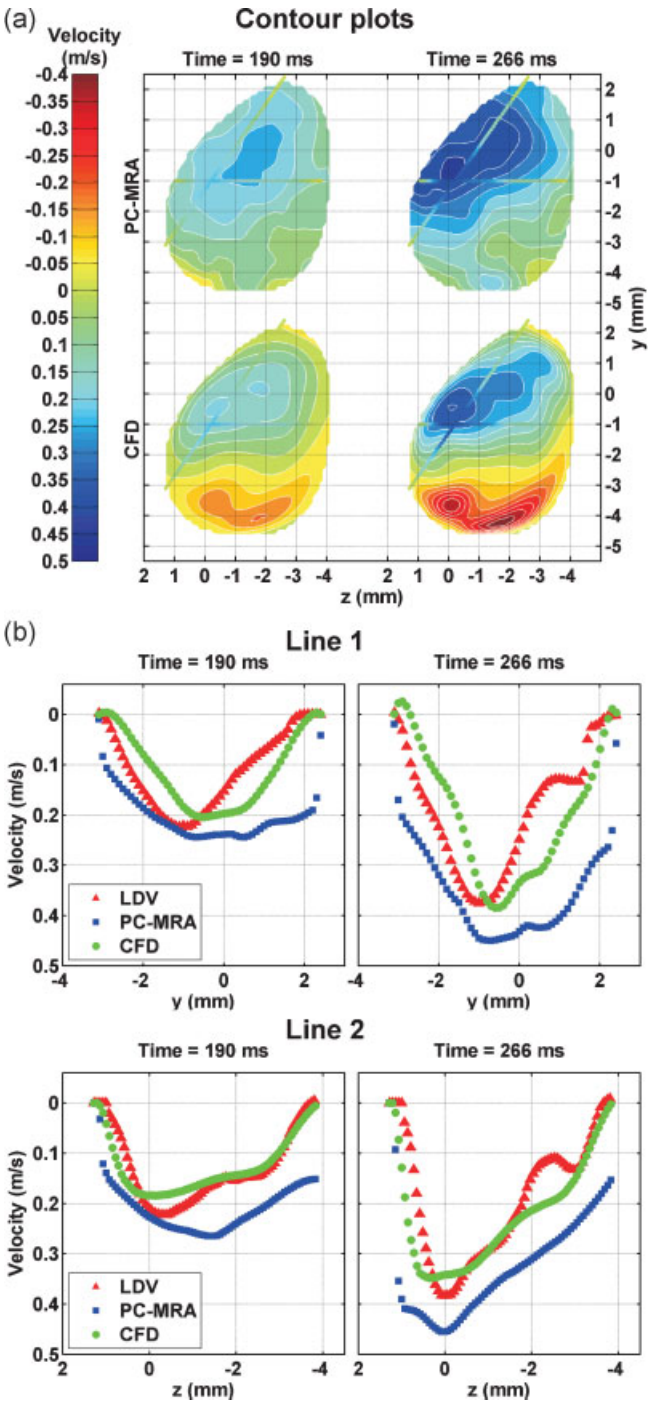

Figure 13. The contour plots (a) of the in-plane velocities in the aneurysm show the PC-MRA and CFD data in the entire cross-section and the lines measured with LDV. In the line plots (b) the extracted data from the PC-MRA and CFD are shown with the lines measured with LDV. It is demonstrated that the velocity values and patterns are similar between all methods, although the PC-MRA values show some differences.

field be sufficiently resolved to capture the salient flow features. Tang *et al*. (38), have recommended obtaining at least 16 isotropic voxels for this purpose. Based on the imaging resolution of 0.49 mm × 0.49 mm provided by PC-MRA acquisition used in our study, a minimum vessel diameter of 2 mm is required for obtaining detailed and reliable results using this method. Indeed, we found the accuracy of PC-MRA to be best in larger vessels (i.e. the internal carotid artery, comprising 50 voxels, and the middle cerebral artery comprising 18 voxels).

Resolution and vessel size are not the only factors that may affect the accuracy of PC-MRA measurements. The obliquity between the long axis of the vessel and the measurement plane is a recognized source of partial volume effects (38), which may be quite severe depending also on the vessel size and the

Table 3. Comparative results of the three different measurement methods on two specific lines within the aneurysm. Percentage-differences from the ideal value and rating as described in the Section 'Analysis'

	Aneurysm					
	PC-MRA–LDV		PC-MRA–CFD		CFD–LDV	
	%	Rating	%	Rating	%	Rating
			Through-plane			
R	19.39	− −	16.82	− −	4.37	+ +
RMSE	17.81	− −	16.67	− −	15.57	− −
m	57.41	− −	53.6	− −	9.45	+
B	−19.15	− −	−19.34	− −	0.85	+ +
PVD	−62.86	− −	−55.12	− −	−7.74	+
MVD	−107.61	− −	−100.54	− −	−7.08	+
Average		−2		−2		+ 0.83
			In-plane			
R	31.63	− −	17.06	− −	16.49	− −
RMSE	17.81	− −	13.64	−	16.47	− −
m	48.96	− −	31.83	− −	23.8	− −
b	59.11	− −	49.14	− −	14.16	−
Average		−2		−1.75		−1.75
			Through-plane and in-plane			
Average		−2		−1.9		−0.2

dimensions of the imaging voxel. The internal carotid artery and middle cerebral artery measurements were performed in regions of an almost straight vessel, whereas the anterior and posterior cerebral arteries had a significant obliquity between the imaging plane and the main flow axis. Moreover, these flow areas could only be covered with 11 and 9 imaging voxels, respectively. Presumably for these reasons the results at these sites were rather poor, despite the diameter of the anterior cerebral artery being of the same order than for the middle cerebral artery. This partial volume effect is reflected in the dispersion of PC-MRA values around the zero velocity, which can be observed at all measurement sites. For the dispersion of the LDV velocities, which is also present, refraction errors of the LDV at places near the arterial wall might play a role. These errors near the wall are less pronounced in CFD, provided that the mesh is adequately fine to resolve the boundary layer, which is an important factor for the accurate calculation of wall shear stresses.

The curvature of natural vessels enforces a degree of secondary flow throughout the circulatory system. An imaging slice not perpendicular to the main velocity direction results in high in-plane velocities, which introduces displacement artifacts due to the non-simultaneity of spatial encoding in PC-MRA, as described by Steinman *et al.* (39). Due to this effect, the measurements of both through-plane and in-plane flow components can be significantly affected. Small in-plane velocities (less than 5% of the through-plane velocities) were present in the internal carotid artery and in the middle cerebral artery, while velocity components of the same order were present in the anterior and posterior cerebral arteries. Our results showed that when the in-plane velocities were small, the through-plane velocities were in better agreement than in the case when in-plane and through-plane velocities were of the same order. The results also showed that in-plane velocity comparisons were always rather poor. Thus, in the cases of the internal carotid and the middle cerebral arteries the very low values of the in-plane velocities, as compared to the through-plane velocities, suggest that they could be neglected. CFD on the other hand corresponded well with LDV measurements for through-plane and higher in-plane velocities, but failed to reproduce very low in-plane velocities.

Within the aneurysm, despite poor quantitative agreement of the measurements obtained with the various methods, a good qualitative agreement was observed related to the conformation of the velocity patterns. Since the aneurysm sac is a region with relatively equivalent velocity components in all three directions, the imaging plane cannot be placed perpendicular to a main flow axis. Partial volume effects and displacement artifacts from the in-plane velocity components are expected to limit the accuracy of velocity measurements. A further consideration is that the size of the voxel volume, in which the PC-MRA obtains its data, is not negligible relative to the scale of the flow features within an aneurysm. This will tend to low-pass filter the spatial depiction of velocity and lead to lower estimates of spatial peak velocity than those obtained with LDV or CFD. In consequence, even with the minimum possible slice thickness of 0.7 mm used here, it seems to be challenging with PC-MRA to obtain detailed 3D velocity data for making precise statements on the velocity patterns within small to middle sized aneurysms as in our model (dimensions of $7 \times 5 \times 5\,\text{mm}^3$).

An important factor in maximizing the VNR is the choice of VENC. The VENC was individually chosen for each measured direction to be high enough for avoiding phase wrapping. To improve the VNR, an alternative would have been to use smaller VENCs and to unwrap the phases as a post-processing step. However, in an aneurysm and for the secondary velocity components in general, the directions of the components are not known beforehand, and may be sufficiently complex, thus leading to an intractable phase unwrapping problem. Multiple measurements

performed with a higher VENC to determine the general direction and a subsequent lower VENC may have reduced the noise, but would have extended the already long measurement times.

In our study, the data were acquired with a *k*-space temporal resolution of 25 ms and interpolated to produce 40 phases over the 500 ms cycle of the pump (reconstructed temporal resolution 12.5 ms). The bilinear interpolation used in this reconstruction can be expected to smoothen the resulting temporal profile for each voxel (40). Based on a Fourier transform of the driving waveform, the power at frequencies above those captured at the acquisition's temporal resolution is expected to be negligible for the specific waveform. Thus, we do not expect significant errors in the net flow. Retrospective triggering is routinely used *in vivo* for flow measurement as it does not introduce transients in the magnetization and eddy currents that can be introduced in prospective sampling by gaps in the excitation train to allow capture of the physiological trigger signal and consistent sampling of each cardiac cycle. The smoothening of the MRA data could be reduced by the use of a prospectively triggered acquisition with sampling extending over more than one cardiac cycle to ensure an entire cardiac cycle can be reconstructed and that a section of the waveform is acquired twice to allow the period affected by transients to be discarded. Such measures would however almost double the scan time required and reduce the SNR of the reconstructed data.

The LDV and CFD measurements are more accurate than the PC-MRA measurements as the spatial and temporal resolution of these methods is much higher than is currently possible with PC-MRA. However, the simulations are sensitive to the geometry and therefore diameter differences between the silicone and the virtual model play a role (41). Since the virtual model was manually segmented from CT measurements of the silicone model, errors due to the CT scan resolution and segmentation could not be avoided. A given mass flow rate in a vessel with a slightly over- or underestimated diameter, would result in lower or higher velocities, respectively. This can be a significant issue for clinical applications where similar or larger errors can be expected during segmentation from clinical MR or CT imaging data obtained from patients, where the scan resolution will be comparable or poorer, or even in DSA, despite the higher resolution of this technique.

In this work, one case of a specific saccular aneurysm was examined. Saccular aneurysms are the most common aneurysms in the circle of Willis. The principles and understandings gained from this case study can be applied also to cases of other aneurysms with different morphology, i.e. a fusiform. The findings showed that the measurements in the feeding arteries provide accurate results. The accuracy should not be influenced by the form of the aneurysm in between. Measurements within the aneurysm however, showed a rather poor depiction of the complex flow patterns, which are likely to be more or less distinctive for different aneurysm geometries.

In general, the flow patterns obtained with PC-MRA, LDV, and CFD were quantitatively in very good concordance. Discrepancies between the methods were most evident in the absolute values of the velocities, in which the CFD simulation tended to over- or underestimate the measured values. The PC-MRA values deviated most from the LDV values close to the time point of peak flow, in the secondary flow component, and in the measurements of low velocities near the vessel wall. Within the aneurysm, the ubiquity of secondary flows, and the presence of low velocities were not well captured by PC-MRA such that at best only a qualitative depiction of the velocity field could be provided with this method. In moderately large, straight vessel segments on the other hand, PC-MRA provided measurements comparable to CFD and in agreement with LDV.

Due to the limitations of PC-MRA in resolving intra-aneurismal flow features and provide reliable estimates of derived quantities, virtual models are needed in small cerebral arteries with aneurysms. Recently, numerical simulations with CFD on realistic arteries and aneurysms became more feasible and offer the possibility to calculate various parameters of the flow field, like velocities, wall shear stresses, and pressure. To take advantage of the benefits of both methods – the patient specific possibilities from the PC-MRA velocity measurements and the possibility to calculate complex flow and pressure parameters in large regions with CFD – a combination seems to be necessary. Thus, accurate, patient specific inlet velocity data are of particular importance as modeling results depend on the inlet flow values. The feeding arteries in the majority of aneurysms located at the circle of Willis are sufficiently large for PC-MRA to provide acceptable levels of measurement accuracy, provided that this technique is applied at a high spatial resolution. Therefore, these values can be used as inlet and outlet conditions for numerical simulations. In smaller arteries and within the aneurysm however, PC-MRA with the present spatial and temporal resolution and SNR constraints can provide at best a qualitative indication of the flow patterns. Further improvement should avoid prolonging the scan time as patient motion is likely to become a limiting factor with longer acquisitions.

In conclusion, time-resolved, retrospectively triggered 3D PC-MRA can provide spatial maps of time dependent velocity components in small arteries with a higher accuracy for rather straight parts of the artery and low in-plane velocities present. As evidenced by our measurements and statistical analyses, the velocity profiles at different sites in the model and at different time instants show a good correspondence between 3D PC-MRA, CFD, and the reference LDV method under these conditions. The achieved results support the use of PC-MRA in providing accurate hemodynamic information for potential use as inlet and outlet conditions in numerical simulations for predicting future aneurismal behavior and treatment planning.

Acknowledgements

Dr Lars Blum, Laboratory of Thermodynamics in Emerging Technologies (LTNT), ETH Zurich, provided assistance with the LDV. Dr Roger Lüchinger, Institute for Biomedical Engineering (IBT), ETH Zurich, kindly helped with the MR scanner. Dr Makoto Ohta, University Hospital Geneva (HUG), supplied the angiographic data. Financial help was provided by Swiss National Science Foundation (SNF), grant number 3200B0-100355.

REFERENCES

1. Chen PR, Frerichs K, Spetzler R. Natural history and general management of unruptured intracranial aneurysms. Neurosurg. Focus 2004; 17(5): E1.
2. King JT Jr. Epidemiology of aneurysmal subarachnoid hemorrhage. Neuroimaging Clin. N. Am. 1997; 7(4): 659–668.
3. Rinkel GJ, Djibuti M, Algra A, van Gijn J. Prevalence and risk of rupture of intracranial aneurysms: a systematic review. Stroke 1998; 29(1): 251–256.

4. Tummala RP, Baskaya MK, Heros RC. Contemporary management of incidental intracranial aneurysms. Neurosurg. Focus 2005; 18(1): e9.
5. Investigators ISUIA. Unruptured intracranial aneurysms–risk of rupture and risks of surgical intervention. N. Engl. J. Med. 1998; 339(24): 1725–1733.
6. Chatziprodromou I, Tricoli A, Poulikakos D, Ventikos Y. Haemodynamics and wall remodelling of a growing cerebral aneurysm: a computational model. J. Biomech. 2007; 40(2): 412–426.
7. Resnick N, Yahav H, Shay-Salit A, Shushy M, Schubert S, Zilberman LC, Wofovitz E. Fluid shear stress and the vascular endothelium: for better and for worse. Prog. Biophys. Mol. Biol. 2003; 81(3): 177–199.
8. Redpath TW, Norris DG, Jones RA, Hutchison JM. A new method of NMR flow imaging. Phys. Med. Biol. 1984; 29(7): 891–895.
9. Bryant DJ, Payne JA, Firmin DN, Longmore DB. Measurement of flow with NMR imaging using a gradient pulse and phase difference technique. J. Comput. Assist. Tomogr. 1984; 8(4): 588–593.
10. Walker MF, Souza SP, Dumoulin CL. Quantitative flow measurement in phase contrast MR angiography. J. Comput. Assist. Tomogr. 1988; 12(2): 304–313.
11. Firmin DN, Nayler GL, Kilner PJ, Longmore DB. The application of phase shifts in NMR for flow measurement. Magn. Reson. Med. 1990; 14(2): 230–241.
12. Ahn S, Shin D, Tateshima S, Tanishita K, Vinuela F, Sinha S. Fluid-induced wall shear stress in anthropomorphic brain aneurysm models: MR phase-contrast study at 3 T. J. Magn. Reson. Imaging 2007; 25(6): 1120–1130.
13. Tateshima S, Grinstead J, Sinha S, Nien YL, Murayama Y, Villablanca JP, Tanishita K, Vinuela F. Intraaneurysmal flow visualization by using phase-contrast magnetic resonance imaging: feasibility study based on a geometrically realistic in vitro aneurysm model. J. Neurosurg. 2004; 100(6): 1041–1048.
14. Tateshima S, Murayama Y, Villablanca JP, Morino T, Takahashi H, Yamauchi T, Tanishita K, Vinuela F. Intraaneurysmal flow dynamics study featuring an acrylic aneurysm model manufactured using a computerized tomography angiogram as a mold. J. Neurosurg. 2001; 95(6): 1020–1027.
15. Hollnagel DI, Summers PE, Kollias SS, Poulikakos D. Laser Doppler velocimetry (LDV) and 3D phase-contrast magnetic resonance angiography (PC-MRA) velocity measurements: validation in an anatomically accurate cerebral artery aneurysm model with steady flow. J. Magn. Reson. Imaging 2007; 26(6): 1493–1505.
16. Urchuk SN, Plewes DB. MR measurements of pulsatile pressure gradients. J. Magn. Reson. Imaging 1994; 4(6): 829–836.
17. Frayne R, Rutt BK. Measurement of fluid-shear rate by Fourier-encoded velocity imaging. Magn. Reson. Med. 1995; 34(3): 378–387.
18. Meckel S, Stalder AF, Santini F, Radu EW, Rufenacht DA, Markl M, Wetzel SG. In vivo visualization and analysis of 3-D hemodynamics in cerebral aneurysms with flow-sensitized 4-D MR imaging at 3 T. Neuroradiology 2008; 50(6): 473–484.
19. Acevedo-Bolton G, Jou LD, Dispensa BP, Lawton MT, Higashida RT, Martin AJ, Young WL, Saloner D. Estimating the hemodynamic impact of interventional treatments of aneurysms: numerical simulation with experimental validation: technical case report. Neurosurgery 2006; 59(2): E429–E430 author reply E429–E430.
20. Cebral JR, Castro MA, Soto O, Lohner R, Alperin N. Blood-flow models of the circle of Willis from magnetic resonance data. J. Eng. Math. 2003; 47(3–4): 369–386.
21. Jou LD, Quick CM, Young WL, Lawton MT, Higashida R, Martin A, Saloner D. Computational approach to quantifying hemodynamic forces in giant cerebral aneurysms. AJNR. Am. J. Neuroradiol. 2003; 24(9): 1804–1810.
22. Steinman DA, Milner JS, Norley CJ, Lownie SP, Holdsworth DW. Image-based computational simulation of flow dynamics in a giant intracranial aneurysm. AJNR. Am. J. Neuroradiol. 2003; 24(4): 559–566.
23. Zhao SZ, Papathanasopoulou P, Long Q, Marshall I, Xu XY. Comparative study of magnetic resonance imaging and image-based computational fluid dynamics for quantification of pulsatile flow in a carotid bifurcation phantom. Ann. Biomed. Eng. 2003; 31(8): 962–971.
24. Rayz VL, Lawton MT, Martin AJ, Young WL, Saloner D. Numerical simulation of pre- and postsurgical flow in a giant basilar aneurysm. J. Biomech. Eng. 2008; 130(2): 021004.
25. Kenner T. The measurement of blood density and its meaning. Basic Res. Cardiol. 1989; 84(2): 111–124.
26. Haynes RH. The Rheology of Blood. T Soc Rheol 1961; 5: 85–101.
27. Merrill EW. Rheology of blood. Physiol. Rev. 1969; 49(4): 863–888.
28. Schmid-Schönbein H, Wells RE, Jr. Rheological properties of human erythrocytes and their influence upon the "anomalous" viscosity of blood. Ergeb. Physiol. 1971; 63: 146–219.
29. Deane CR, Markus HS. Colour velocity flow measurement: in vitro validation and application to human carotid arteries. Ultrasound Med. Biol. 1997; 23(3): 447–452.
30. Ho SS, Metreweli C. Preferred technique for blood flow volume measurement in cerebrovascular disease. Stroke 2000; 31(6): 1342–1345.
31. Soustiel JF, Levy E, Zaaroor M, Bibi R, Lukaschuk S, Manor D. A new angle-independent Doppler ultrasonic device for assessment of blood flow volume in the extracranial internal carotid artery. J. Ultrasound Med. 2002; 21(12): 1405–1412.
32. Schebesch KM, Simka S, Woertgen C, Brawanski A, Rothoerl RD. Normal values of volume flow in the internal carotid artery measured by a new angle-independent Doppler technique for evaluating cerebral perfusion. Acta Neurochir. (Wien) 2004; 146(9): 983–986 discussion 986–987.
33. Scheel P, Ruge C, Schoning M. Flow velocity and flow volume measurements in the extracranial carotid and vertebral arteries in healthy adults: reference data and the effects of age. Ultrasound Med. Biol. 2000; 26(8): 1261–1266.
34. Holdsworth DW, Rickey DW, Drangova M, Miller DJ, Fenster A. Computer-controlled positive displacement pump for physiological flow simulation. Med. Biol. Eng. Comput. 1991; 29(6): 565–570.
35. Frayne R, Holdsworth DW, Gowman LM, Rickey DW, Drangova M, Fenster A, Rutt BK. Computer-controlled flow simulator for MR flow studies. J. Magn. Reson. Imaging 1992; 2(5): 605–612.
36. Durst F, Melling A, Whitelaw JH. *Principles and Practice of Laser-Doppler Anemometry*. Academic Press: London, 1981; 437.
37. DANTEC. *Burst Spectrum Analyser, User's guide*. DANTEC Electronics: Skovlund, Denmark, 1990.
38. Tang C, Blatter DD, Parker DL. Accuracy of phase-contrast flow measurements in the presence of partial-volume effects. J. Magn. Reson. Imaging 1993; 3(2): 377–385.
39. Steinman DA, Ethier CR, Rutt BK. Combined analysis of spatial and velocity displacement artifacts in phase contrast measurements of complex flows. J. Magn. Reson. Imaging 1997; 7(2): 339–346.
40. Frayne R, Rutt BK. Frequency response to retrospectively gated phase-contrast MR imaging: effect of interpolation. J. Magn. Reson. Imaging 1993; 3(6): 907–917.
41. Ford MD, Nikolov HN, Milner JS, Lownie SP, Demont EM, Kalata W, Loth F, Holdsworth DW, Steinman DA. PIV-measured versus CFD-predicted flow dynamics in anatomically realistic cerebral aneurysm models. J. Biomech. Eng. 2008; 130(2): 021015.